Edge Detection of Real Synthetic Aperture Radar Images through Filtered Back Projection

Noe Pena, Guillermo Garza, Yufeng Cao, and Zhijun Qiao
Department of Mathematics, University of Texas-Pan American,
1201 W. University Dr., Edinburg, TX 78539 USA
Email: qiao@utpa.edu

***Abstract*—Detecting edges is an important task in processing images in order to see objects from SAR data. In this work, the received data is first filtered and then back-projected. The edges are detected in both the x and y directions and results shown. SAR segmented images generated using this technique, are provided from a publicly available SAR data set. In our work, this technique is applied on real SAR data with significant results.**

***Index Terms*—Synthetic Aperture Radar, Back-projection, Edge Detection, Imaging**

I. INTRODUCTION

In SAR imaging an antenna sends electromagnetic waves and the scattered waves are detected. Using the method proposed by[6] in the reconstruction of images, edges can be detected to try and identify objects in the scene. This process has many applications, especially now that identification is so important.

Edge detection in images is an important task used to locate and describe objects within that image. Usual methods for edge detection are Canny, Prewitt, and Sobel. These stated methods work after the image has been formed. The method proposed by[6] does edge detection by applying a differential filter directly to the SAR data at the backprojection step.

In most areas of SAR the received signal model is derived from Maxwell's equations. The derivation is a very important step that must be taken by anyone studying radar. A complete understanding can help to find better ways to model this in the future. This can also lead to different methods of image reconstruction.

In this paper, the mathematical model for reconstructing images is reviewed and the process of edge detection defined by[6] is implemented on a real SAR dataset. The method detects edges from the received signal before regular image reconstruction. New Matlab code was written following[5], [11] combined with this edge detection method to produce images with edges which are well defined. Then applying a thresholding algorithm, the final image is produced.

This paper is organized as follows: In Section 2, the SAR received signal is modelled, the forward model and Filtered Backprojection method are shown, and the edge detection method[6] is discussed. In Section 3, the experiments and results are outlined and presented. Finally, the discussion is concluded in Section 4.

II. MATHEMATICAL MODEL

In this section the origin of the received signal $r(s,t)$ model is reviewed following a version of[7], and the forward model and filtered backprojection is derived. It is important to re-establish these models for persons not completely familiar with this area.

A. Wave Propagation

The scalar wave equation

$$(\nabla^2 - \frac{\partial_t^2}{c^2(x)})U(t,x) = 0 \tag{1}$$

(where the function c is the wave propagation speed) is commonly used for SAR. This model works very well for the propagation of electromagnetic waves in dry air. It is assumed that the target is a sufficient distance from the radar and that in dry air $c(x) = c_0$ (where c_0 is the speed of light in vacuum).

B. Field from an Antenna

The field emanating from an antenna U^{in} satisfies

$$(\nabla^2 - \frac{\partial_t^2}{c_0^2(x)})U^{in}(t,x) = -P(t)J_s(x) \tag{2}$$

where

$$U^{in}(t,x) = \int \frac{P(t - |x-y|/c_0)}{4\pi |x-y|} J_s(y)dy. \tag{3}$$

Here J_s is the time derivative of the current distribution over the antenna, and $P(t)$ is the waveform sent to the antenna. Writing P in terms of its Fourier transform p, (3) becomes

$$U^{in}(t,x) = \int \frac{e^{-i\omega(t-|x-y|/c_0)}}{4\pi |x-y|} p(\omega)J_s(y)d\omega dy. \tag{4}$$

C. Far-Field Approximation

The assumption that the size of the antenna is much smaller than the distance from the target location x to center of the antenna y_0 is made. So $|y-y_0| \ll |x-y_0|$ where y is a point on the antenna. Then

$$|x-y| = |x-y_0| - \widehat{(x-y_0)} \cdot (y-y_0) + O(\frac{|y-y_0|^2}{|x-y_0|}) \tag{5}$$

978-1-4673-0199-2/12/$31.00 ©2012 IEEE

is called the far field expansion. It makes use of the definition of absolute value and the Taylor expansion $\sqrt{1+a} = 1 + \frac{a}{2} + O(a^2)$. Using (5) in (4)

$$U^{in}(t,x) \approx \int \frac{e^{-i\omega(t-|x-y_0|/c_0)}}{4\pi|x-y_0|} \times e^{-i\omega\widehat{(x-y_0)}\cdot(y-y_0)} p(\omega) J_s(y) d\omega dy \quad (6)$$

is obtained.

D. Scattering Model

The model used for wave propagation including the source is

$$(\nabla^2 - \frac{\partial_t^2}{c^2(x)})U(t,x) = -P(t)J_s(x). \quad (7)$$

Using the fact that $U = U^{in} + U^{sc}$, (2) and some algebra, (7) becomes

$$(\nabla^2 - \frac{\partial_t^2}{c_0^2(x)})U^{sc}(t,x) = -V(x)\partial_t^2 U(t,x) \quad (8)$$

where

$$V(x) = \frac{1}{c_0^2} - \frac{1}{c^2(x)}.$$

This V is called the reflectivity function. Its discontinuities are what need to be recovered. Writing (8) as an integral equation,

$$U^{sc}(t,x) = \int \frac{\delta(t-\tau-|x-z|/c_0)}{4\pi|x-z|} V(z)\partial_t^2 U(\tau,z) d\tau dz \quad (9)$$

then using the Born approximation and evaluating the integral with respect to τ

$$U^{sc}(t,x) \approx \int \frac{\delta(t-\tau-|x-z|/c_0)}{4\pi|x-z|} V(z)\partial_t^2 U^{in}(\tau,z) d\tau dz$$

$$= \int \frac{V(z)}{4\pi|x-z|} \partial_t^2 U^{in}(t-|x-z|/c_0, z) dz \quad (10)$$

is obtained.[7] This approximation basically replaces the full field by the incident field. Now evaluating the partial derivative and using (6), converts (10) into

$$U^{sc}(t,x) \approx \int \frac{e^{-i\omega((t-(|x-z|+|z-y_0|)/c_0))}}{(4\pi)^2|x-z||z-y_0|} \omega^2 \times p(\omega) e^{-i\omega\widehat{(z-y_0)}\cdot(y-y_0)} J_s(y) V(z) d\omega dz$$

At $x = y_0$ we have

$$U^{sc}(t,y_0) \approx \int \frac{e^{-i\omega((t-2|z-y_0|/c_0))}}{(4\pi)^2|z-y_0|^2} \omega^2 p(\omega) \times e^{-i\omega\widehat{(z-y_0)}\cdot(y-y_0)} J_s(y) V(z) d\omega dz. \quad (11)$$

Parametrizing the surface by $\gamma := \{\gamma(s) : s_{min} < s < s_{max}\}$[9] and denoting the map from the scene V to data r by $\mathcal{F}$ the received signal is modeled following [7]

$$r(s,t) = \mathcal{F}[V](s,t) = \int e^{-i2\pi\omega(t-R(s,\mathbf{x})/c_0)} \times A(\boldsymbol{x},\omega,s) V(\boldsymbol{x}) d\omega d\boldsymbol{x}, \quad (12)$$

where $R(s,\mathbf{x}) = 2|\mathbf{x}-\gamma(s)|$ with $\gamma(s), \mathbf{x}\epsilon\mathbb{R}^3, \boldsymbol{x}\epsilon\mathbb{R}^2$, and roman small letters in $\mathbb{R}$. An assumption is made that the amplitude A of (12) satisfies

$$\sup_{(s,\boldsymbol{x})\epsilon K} \left|\partial_\omega^\alpha \partial_s^\beta \partial_{x_1}^{\rho_1} \partial_{x_2}^{\rho_2} A(\boldsymbol{x},\omega,s)\right| \leq C_0(1+\omega^2)^{(m_A-|\alpha|)/2}$$

where K is any compact set. This assumption makes the forward operator $\mathcal{F}$ a $Fourier\ Integral\ Operator$ (FIO)[6]

E. Filtered-Backprojection

Here $V(\boldsymbol{x})$ is reconstructed by inverting $\mathcal{F}$ with another FIO $\mathcal{K}$ such that the kernel of $\mathcal{K}\mathcal{F}$ is approximately a Dirac delta function.[8] So the operator $\mathcal{K}$ is designed to reconstruct the image according to.[7] Hence the reconstructed image $V(\boldsymbol{z})$ is

$$V(\boldsymbol{z}) \approx \mathcal{K}[r](\boldsymbol{z}) = \int e^{i2\pi\omega(t-R(s,\mathbf{z})/c_0)} Q(\boldsymbol{z},\omega,s) r(s,t) d\omega ds dt. \quad (13)$$

Therefore the $point\ spread\ function$ T of $\mathcal{K}$ is

$$T(\boldsymbol{z},\boldsymbol{x}) = \int e^{i2\pi\omega(R(s,\mathbf{x})-R(s,\mathbf{z}))/c_0} Q(\boldsymbol{z},s,\omega) A(\boldsymbol{x},s,\omega) d\omega ds \quad (14)$$

where it is common to choose Q such that $T(\boldsymbol{z},\boldsymbol{x})$ is a delta function, but for edge detection Q' must be obtained according to.[6]

F. Edge detection of SAR Data

Here the matched filter Q' is obtained following.[6] But first according to[9]

$$V(\boldsymbol{z}) \approx \int_{\Omega_z} e^{i2\pi(\boldsymbol{x}-\boldsymbol{z})\cdot\boldsymbol{\xi}} \chi_{\Omega_z}(\boldsymbol{\xi}) V(\boldsymbol{x}) d\boldsymbol{x} d\boldsymbol{\xi} \quad (15)$$

where $\Omega_z = \{\boldsymbol{\xi}(\omega,s,z) | A(z,s,\omega) \neq 0\}$ and χ_{Ω_z} is a smooth cut off function equal one in the interior of Ω_z and zero in the exterior. Then[6] defines the filter Q' generally as

$$Q'(\boldsymbol{\xi}) = \sum_i \alpha_i \left|\hat{\boldsymbol{\mu}}_{p_i} \cdot \boldsymbol{\xi}\right|^{p_i}$$

where $\alpha_i > 0$ and $p_i \epsilon \mathbb{R}$. So the $point\ spread\ function$ of the edge detecting reconstruction operator is

$$T(\boldsymbol{z},\boldsymbol{x}) \approx \sum_i \alpha_{p_i} \int e^{i2\pi(\boldsymbol{z}-\boldsymbol{x})\cdot\boldsymbol{\xi}} \left|\hat{\boldsymbol{\mu}}_{p_i} \cdot \boldsymbol{\xi}\right|^{p_i} d\boldsymbol{\xi}. \quad (16)$$

Since this filter helps control directions of what needs to be enhanced, in this paper scenes are reconstructed in this manner.

III. EXPERIMENTS

In these experiments the process described above is written into Matlab code written by[5] to be able to detect the edges from two data sets. The first data set is the "Gotcha Volumetric SAR Data Set, Version 1.0," consisting of SAR phase history data collected at X-band with a 640 MHz bandwidth with full azimuth coverage at 8 different elevation angles with full polarization. The second data set is the "Civilian Vehicle Radar Data Domes" dataset consisting of simulated X-band scattering data for civilian vehicles.

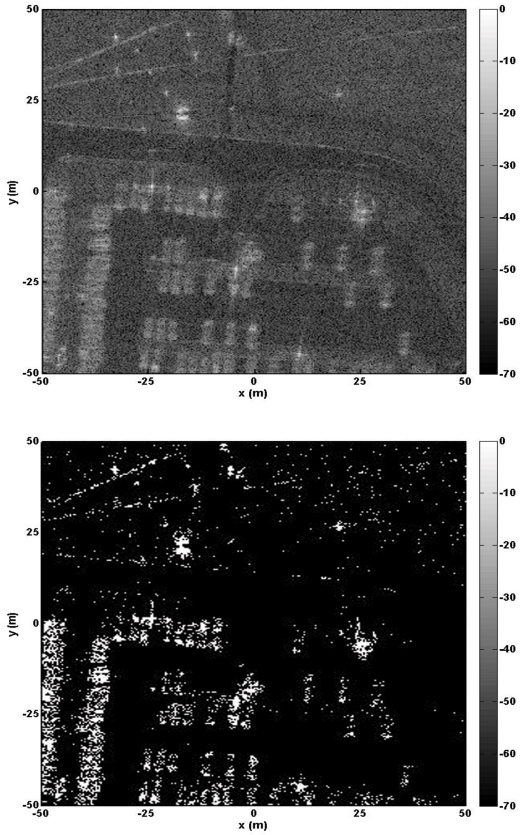

Fig. 1. *Enhancement of edges in y-direction for first dataset.(Left)Reconstructed image with p=1, α=0.7.(Right)Thresholded image with intensity=.47*

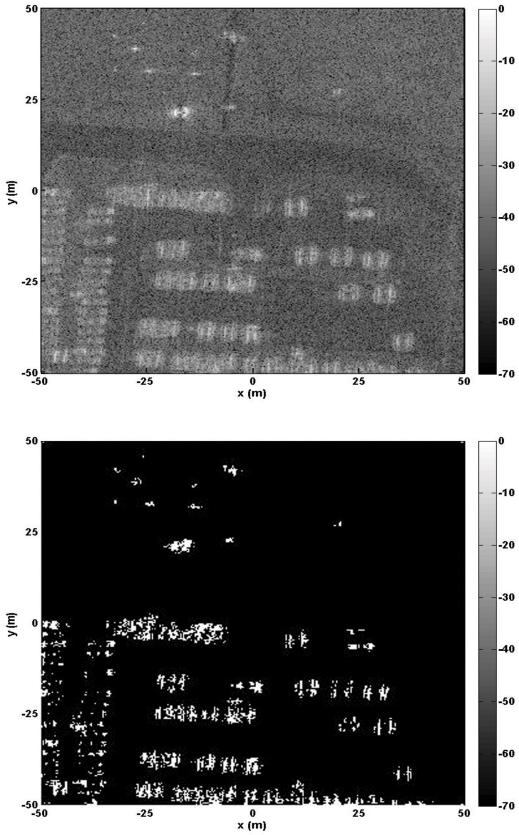

Fig. 2. *Enhancement of edges in x-direction for first dataset.(Left)Reconstructed image with p=2, α=0.8.(Right)Thresholded image with intensity=.51.*

For the first data set the scene is imaged with edges enhanced in all directions, the x-direction only (with $\mu = (1, 0)$ in (16)), and the y-direction only (with $\mu = (0, 1)$. For the second dataset three vehicles were imaged. The Toyota Camry, Jeep, and the Toyota Tacoma served this experiment. The figures show reconstructed (part a) and thresholded (part b). The iterative thresholding method proposed by[6] is used with some minor changes.

IV. CONCLUSIONS

The edge detection method used here worked with both datasets without very much difficulty. Currently, this method is being implemented on other datasets and synthetic data. This work has shown that the method defined by[6] works on real datasets as well as synthetic datasets. It is important to note that much work is still needed in edge detection in the presence of clutter and noise. In future work it will be discussed how statistical methods can improve the image reconstruction in the presence of clutter and noise.

ACKNOWLEDGMENTS

This work was partially supported by the US Department of Defense Army Research Office under grant number *W911NF-08-1-0511*, and by the Norman Hackerman Advanced Research Program under grant number *003599-0001-2009*.

REFERENCES

[1] Casteel C., Gorham L. et al, Minardi M., Scarborough S., Naidu K., "A challenge problem for 2D/3D imaging of targets from a volumetric data set in an urban environment," *Algorithms for Synthetic Aperture Radar Imagery XIV, Proc. SPIE* **6568**, 2007.

[2] Garza G., "Mathematics of Synthetic Aperture Radar," *Master's Thesis*, University of Texas - Pan American, 2011.

[3] Guillermo Garza and Zhijun Qiao, Resolution analysis of bistatic SAR, Proceedings of SPIE Vol. 8021, 802169, 2011.

[4] Guillermo Garza, Jaime Lopez, and Zhijun Qiao, Cross-range imaging of SAR and PDE analysis, Proceeding of SPIE Vol. 7698 76981C-1-C15, 2010.

[5] Gorham L. A. and Moore, L. J., "SAR image formation toolbox for MATLAB," *Algorithms for Synthetic Aperture Radar Imagery XVII* **7669**, *SPIE*, 2010.

[6] Yanik, H. C., Zhengmin L., and Yazici, B., "Computationally Efficient FBPtype Direct Segmentation of Synthetic Aperture Radar Images, *Algorithms for Synthetic Aperture Radar Imagery XVII, Proc. SPIE* **8051**, 2011.

[7] Nolan, C. J. and Cheney, M., "Synthetic Aperture Inversion," *Inverse Problems* **18**, 221-235, 2002.

[8] Yarman, C. E., Yazici, B., and Cheney, M., "Bistatic Synthetic Aperture Radar Imaging for Arbitrary Flight Trajectories," *IEEE Transactions on Image Processing*, Vol. **17**, No. 1, pp. 84-93, Jan. 2008.

[9] Yarman, C. E., Yazici, B., and Cheney, M., "Bistatic Synthetic Aperture Radar Imaging for Arbitrary Flight Trajectories and Non-flat Topography," *IEEE Radar Conference 2007*, pp. 712-716, 17-20 April 2007.

[10] Willis, N. J., *Bistatic Radar*. Norwood, MA: Artech House, 1991.

[11] Dungan, K. E., et al,"Civilian Vehicle Radar Data Domes," *Algorithms for Synthetic Aperture Radar Imagery XVII* **7669**, *SPIE*, 2010.

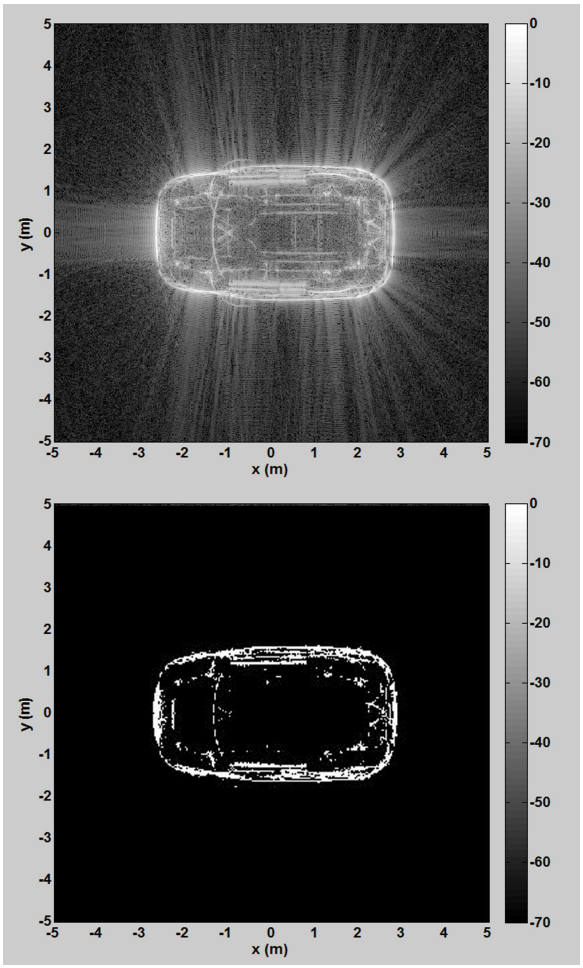

Fig. 3. *Jeep Grand Cherokee with edges enhanced in all directions from second dataset.(Left)Reconstructed image with p=1, α=0.8.(Right)Thresholded image with intensity=.70*

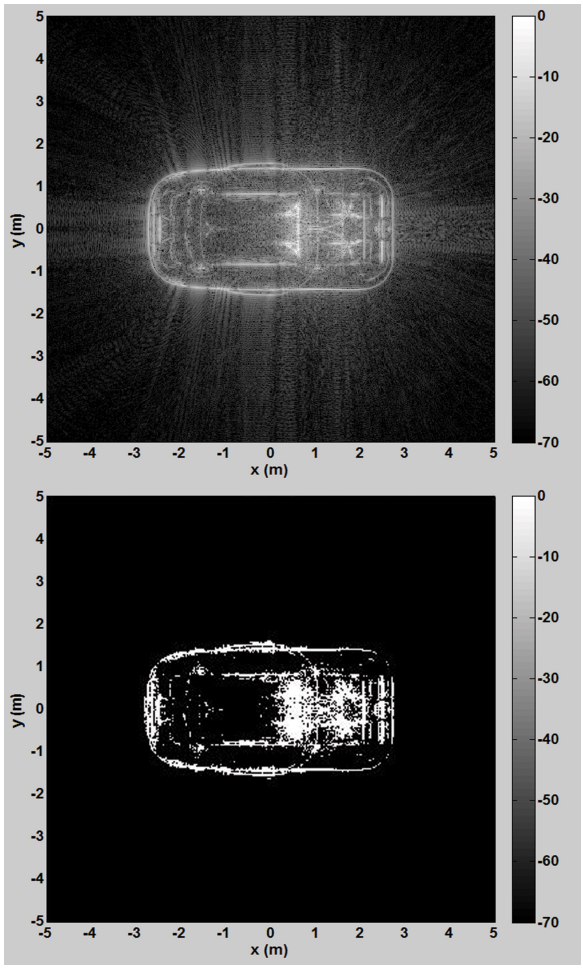

Fig. 4. *Toyota Tacoma with edges enhanced in all directions from second dataset.(Left)Reconstructed image with p=1, α=0.8.(Right)Thresholded image with intensity=.53*